IEEE Access
Multidisciplinary | Rapid Review | Open Access Journal

Received 6 June 2024, accepted 9 July 2024, date of publication 15 July 2024, date of current version 24 July 2024.

Digital Object Identifier 10.1109/ACCESS.2024.3427671

RESEARCH ARTICLE

Nonlinear Robust Control of a Differential Boost Inverter Based on Disturbance Compensation and Additional Sliding-Mode Component

ANTONINO SFERLAZZA[1], (Senior Member, IEEE), SILVIA DI GIROLAMO[1], (Student Member, IEEE), GIOVANNI GARRAFFA[2], (Member, IEEE), FRANCESCO ALONGE[1], (Life Member, IEEE), IVAN MARCHESE[1], VINCENZO LEONARDI[3], FRANCESCO MARIA RAIMONDI[1], AND FILIPPO D'IPPOLITO[1], (Senior Member, IEEE)

[1]Department of Engineering, University of Palermo, 90128 Palermo, Italy
[2]Department of Engineering and Architecture, Kore University of Enna, 94100 Enna, Italy
[3]TopNetwork SpA, 90143 Palermo, Italy

Corresponding author: Giovanni Garraffa (giovanni.garraffa@unikore.it)

This work was supported in part by European Union (NextGeneration EU), through Ministero dell'Università e della Ricerca (MUR)-Piano Nazionale di Ripresa e Resilienza (PNRR) Project SAMOTHRACE (ECS00000022)–CUP: B73C22000810001.

ABSTRACT This paper deals with the nonlinear robust PWM control of a DC/AC differential boost inverter based on dynamic feedback linearization, active disturbance rejection, and sliding mode control techniques. The inverter topology consists of two synchronous boost converters linked through a load resistance. The model of each boost converter is put in Brunovski's canonical form through dynamic feedback linearization, defining an auxiliary input depending on the control variable in an affine mode and a nonlinear disturbance containing endogenous and exogenous variables. Each disturbance is estimated by an extended state observer and compensated through a control law designed for tracking the desired trajectory, according to the active disturbance rejection control technique. Finally, a sliding mode component is designed and added to the previous control law to assure the robustness of the closed loop system against uncertainties due to electric parameters, supply voltage and load resistance deviations, and disturbance estimation errors. Experimental results validate the proposed control methodology.

INDEX TERMS Boost inverter, dynamic feedback linearization, sliding mode control, trajectory tracking.

I. INTRODUCTION

The scientific literature widely addresses the control of boost DC/DC and DC/AC converters using various model-based control methods. The boost converter, usually employed in DC/DC applications, can also be used for directly converting a DC input voltage into a sinusoidal AC voltage with assigned amplitude and frequency superimposed on a mean value different from zero (see, for example, [1], [2]). However, many applications require that the sinusoidal voltage have a mean value equal to zero. This task can be accomplished using a converter topology named Differential Boost Inverter (DBI), consisting of two synchronous boost converters connected through a load, as proposed and discussed in [3]. Concerning the control techniques employed for this boost inverter, it is convenient to mention those based on the small-signal linearized model (cf., for example, [3], [4], [5], [6], [7]), which employ control methods based on the transfer function, and those based on the Sliding Mode (SM) technique (cf., for example, [8], [9], [10], [11], [12], [13] and [14]) based on the state space model. A recent interesting overview of differential single-phase inverter topologies with active power decoupling and their main control techniques is given in [15].

In [3], the controller for each boost converter is designed starting from a mathematical model of the boost converter. A transfer function is obtained by linearizing this mathematical model, and a controller is designed in the frequency

The associate editor coordinating the review of this manuscript and approving it for publication was Snehal Gawande.

domain. The controller is implemented via a hardware circuit consisting of an operational amplifier and an RC network. In [4], the same approach is followed, designing two control loops for each boost; the outer loop gives the reference current for the inner loop, and the inner loop gives the duty cycle. Both loops are controlled using PI controllers. In [5], a fractional order PID-type control algorithm for a boost converter is proposed. A suitable procedure for computing the parameters of the fractional controller is given, together with a discretizing method for implementing it in a floating-point DSP. In [6], a new topology of a fractional order PID controller is proposed to control a boost converter with minimum over/undershoot. The fractional controller parameters are tuned using a genetic algorithm with a combined cost function composed of the integral of time-weighted absolute error (ITAE) and time-weighted square error (ITSE). In [7], the problem of generating a sinusoidal waveform at high frequency is addressed. It is shown that using a particular nonlinear feedback linearization technique, it is possible to generate a sinusoidal waveform at 2 kHz using the DBI topology mentioned above.

By considering the sliding mode techniques, in [8], the controller for each boost converter is designed according to the sliding mode control method, assuming as a sliding function a linear combination of the tracking errors of the reference current and voltage. While the reference voltage is well-defined, the reference current is not an exogenous well-defined signal, and this current is assumed to be the output of a high-pass filter. The implementation of the controller is carried out via hardware through an electronic circuit. In [9], a sliding mode controller is designed for the whole system, assuming that only two configurations occur among the four conduction configurations of the DBI converter. The sliding function is chosen according to the current-mode design method, and the controller is implemented at a constant frequency using the equivalent control corresponding to the chosen sliding function. In [10], a two loops control system is illustrated, where the inner loop is controlled using the sliding mode method with the same sliding function as in [9], the outer loop is PI-type and gives the reference signal for the inner loop so that the output voltage error converges to zero. In [11], a global sliding mode current control scheme for a grid-connected DBI is presented. In [12], the controller for the boost converter is designed according to the sliding mode control based on switched capacitors with high DC gain and low voltage stress. In [13], a sliding-mode backstepping control is proposed for boost converters in real-time for LED lighting applications. The sliding surface in the backstepping control procedure ensures the robustness of the system by attaining an asymptotically stable system. A sliding mode backstepping controller is formulated to tackle uncertainties caused by load and input supply variations. In [14], a control law is proposed in terms of the duty cycle. This law is derived by employing the dynamic sliding mode control method applied to the conventional averaged model, where the control variables are the duty cycles; the sliding function is obtained according to the current mode method, adding a term proportional to the integral of the tracking voltage error. For each boost converter, the duty cycle consists of two terms: a continuous term given by the equivalent control corresponding to the chosen sliding function and a discontinuous term proportional to the sign of the sliding function itself.

In this paper, a PWM controller for a DBI is designed. The controller is obtained by combining advanced methodologies, such as state feedback linearization, active disturbance rejection control, and sliding mode control. The state feedback linearization puts the nonlinear model into the linear Brunovski canonical form; the ADRC approach allows the estimate of the disturbance present in the linearized model, and, finally, the SM control is aimed at gaining robustness against possible disturbance estimation errors. This idea signifies the difference between other works present in literature where the control of a boost inverter is never analyzed using the ADRC with an additional sliding mode component. The controller is designed starting from the nonlinear averaged state-space mathematical model with two independent control variables consisting of the duty cycles of the two converters. Although the whole controller is more complex than those considered in [9], it is more versatile because it can manage all the possible conduction configurations of the converter, and then it is possible to control the two boost converters separately. Moreover, it can be directly implemented using PWM control methods, thus avoiding deterioration of the regulation properties produced by the transformation from the sliding mode controller into the PWM one as in [16].

More in details, in this work, the model of each boost converter is put in Brunovski's canonical form through dynamic feedback linearization [17], defining an auxiliary input depending on endogenous and exogenous variables. Each disturbance is estimated by an extended state observer and compensated through a control law designed for tracking the desired trajectory, according to the active disturbance rejection control technique. Furthermore, a sliding mode component is designed and added to the previous control law to assure the robustness of the closed loop system against uncertainties due to electric parameters, supply voltage, load resistance deviations, and disturbance estimation errors. The control law for trajectory tracking requires knowledge of the derivatives of currents, which is carried out using two linear differentiators. The proposed control technique is tested both by simulations and experimentally, and the results show its feasibility and reliability.

A. COMPARISON WITH THE CURRENT LITERATURE

Other recent literature works deal with the active disturbance rejection control of converters [18], [19], [20], [21], [22], [23], [24], [25]. However, they deal with a single boost for DC/DC applications, and it has never been applied in a DBI configuration. Moreover, they do not consider the additional

sliding mode component design included in the proposed technique, which allows for better robustness against a mismatch of the electric parameters, parametric deviations, and input voltage and load variations, as better described in the paper.

By comparing our paper with other dynamic sliding mode techniques already presented in the literature, some relevant differences exist. Indeed, the proposed control method is based on the active compensation of the disturbances (both endogenous and exogenous), and, differently from previously cited papers about sliding mode control ([8], [9], [10], [11], [13], [14]), here the dynamic control method is achieved by extending the state, including the duty-cycle, and defining an auxiliary control variable which is the derivative of the duty-cycle itself. Therefore, the sliding mode component is added to this auxiliary control variable instead of the duty cycle, which implies that problems due to the chattering are highly attenuated because the discontinuous component is filtered out by an integration stage; those avoiding the implementation of suitably designed filters like in [14]. Finally, the validity of the proposed law is not limited to small signal variations, and it assures a good tracking of the desired output trajectory, no distortions, and adequate robustness property.

In summary, the proposed control technique combines the benefits of the active disturbance rejection control (never applied to the DBI) to generate a robust control where the equivalent disturbances are online estimated and compensated, with the benefits of the sliding mode control to make the system robust against uncertainties on the input gain and other exogenous disturbances acting in the input. Moreover, by means of the dynamic input, the chattering problems of the sliding mode control are overcome. This combined configuration has never been applied to DBI to the best of the Author's knowledge, and it is very promising from the robustness point of view, as will be shown from the results given in this paper.

II. DYNAMIC MODEL OF THE DBI AND PROBLEM STATEMENT

The electrical circuit of the boost inverter is shown in Fig. 1. The differential equations describing the dynamics of the boost inverter can be written using the averaged state-space mathematical model [26] as follows:

$$\dot{i}_{L_1} = -\frac{1}{L_1}(1-\lambda_1)v_{C_1} + \frac{1}{L_1}V_{in}, \tag{1a}$$

$$\dot{v}_{C_1} = -\frac{1}{RC_1}(v_{C_1} - v_{C_2}) + \frac{1}{C_1}(1-\lambda_1)i_{L_1}, \tag{1b}$$

$$\dot{i}_{L_2} = -\frac{1}{L_2}(1-\lambda_2)v_{C_2} + \frac{1}{L_2}V_{in}, \tag{1c}$$

$$\dot{v}_{C_2} = -\frac{1}{RC_2}(v_{C_2} - v_{C_1}) + \frac{1}{C_2}(1-\lambda_2)i_{L_2}, \tag{1d}$$

where i_{L_1} and i_{L_2} are the inductor currents flowing in the inductors L_1 and L_2, respectively, v_{C_1} and v_{C_2} are the voltages on the capacitors C_1 and C_2, respectively, V_{in} is the DC supply voltage and R is the load resistance. Moreover, λ_1 and λ_2 represent the duty cycles. In particular, by defining a modulation period equal to T_{PWM}, the switches S_1 and S_4 are managed by considering a turn-on period equal to $T_{1,ON} = \lambda_1 T_{PWM}$ for S_1 and $T_{2,ON} = \lambda_2 T_{PWM}$ for S_4; while the turn off period is, respectively, $T_{1,OFF} = (1-\lambda_1)T_{PWM}$ and $T_{2,OFF} = (1-\lambda_2)T_{PWM}$. The switches S_2 and S_3 are managed in a complementary way concerning S_1 and S_4. Note that the parasitic resistances of inductors and capacitors have been neglected, and the assumption of continuous conduction mode has been considered.

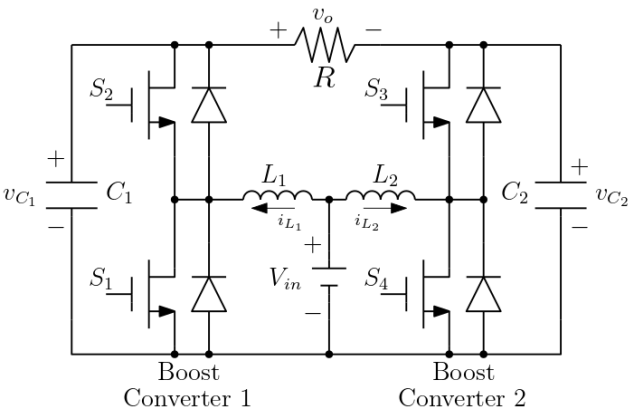

FIGURE 1. Scheme of the differential boost inverter.

The main goal of this work is to design a controller for the DBI so that the output voltage v_o, defined as:

$$v_o = v_{C1} - v_{C2}, \tag{2}$$

tracks a sinusoidal reference (i.e., $v_o = V_o \sin(\omega_o t)$), rejecting both exogenous and endogenous disturbances and ensuring the robustness and stability of the closed loop system. Note that the DBI can be considered like two coupled synchronous boost converters (indicated in Fig. 1 as boost converter 1 and boost converter 2) sourced from the same input. To simplify the notation, the synchronous boost converter 1 (left side) will be indicated with Boost-1, and the synchronous boost converter 2 (right side) will be indicated with Boost-2. It is helpful to observe that equations (1a) and (1b) constitute the model of the Boost-1, where the interaction with Boost-2 is represented by the variable v_{C2}, whereas the model of the Boost-2 is given by (1c) and (1d), where the interaction with Boost-1 is due to v_{C1}. Based on this consideration, the above-described goal can be modified by considering the control of these two boost converters separately and their interactions. For this reason, the following desired output voltages, v^*_{C1} and v^*_{C2}, for the two converters will be considered:

$$v^*_{C1} = V_{dc} + \frac{V_o}{2}sin(\omega_o t), \tag{3}$$

$$v^*_{C2} = V_{dc} - \frac{V_o}{2}sin(\omega_o t), \tag{4}$$

where V_{dc} is the mean output voltage value that ensures the continuous conduction mode (i.e., $V_{dc} > \frac{V_o}{2}$).

III. DESIGN OF THE CONTROL ALGORITHM

The main idea is to control Boost-1 and Boost-2 separately and adequately manage their interactions. Each converter will be controlled through the active disturbance rejection technique, where the interaction effects between the two converters are considered exogenous disturbances and can be estimated by an extended state observer (ESO) and compensated. More precisely, the active disturbance rejection approach is based on constructing an extended model of order $n+1$, where n is the order of the controlled system, by defining an additional state variable representing the total disturbance.

This model is then employed to design an ESO to estimate the total disturbance. Finally, starting from the above-controlled system model of order n, the control law consists of two components: the first compensates for the total disturbance, and the second assigns the desired behaviors and assures the desired robustness property. Since the two converters share the same structure, only one controller will be addressed. Let us consider the Boost-1. To apply the active disturbance technique, it is necessary to express the extended model in the Brunovsky's canonical form, as shown below.

A. THE BRUNOVSKY'S CANONICAL FORM WITH INTEGRAL DYNAMIC INPUT

According to [27], the Brunovsky's canonical form can be obtained by defining a variable δ_1, such that

$$\dot{\lambda}_1 = \delta_1, \tag{5}$$

where δ_1 is considered an auxiliary input for Boost-1. Then, defining the variable:

$$z_1 := C_1 v_{C_1}^2 + L_1 i_{L_1}^2, \tag{6}$$

i.e. the flat output (cf. for example [1]), it is possible to consider a new state vector given by:

$$\boldsymbol{z} = \begin{bmatrix} z_1 & z_2 & z_3 \end{bmatrix}^\top = \begin{bmatrix} z_1 & \dot{z}_1 & \ddot{z}_1 \end{bmatrix}^\top, \tag{7}$$

where

$$z_2 = 2V_{in} i_{L_1} - \frac{2}{R} v_{C_1}(v_{C_1} - v_{C_2}), \tag{8}$$

$$\begin{aligned} z_3 = {} & \frac{2}{R^2 C_1}(v_{C_1} - v_{C_2})(2v_{C_1} - v_{C_2}) + \frac{2}{RC_2} v_{C_1}\left[\frac{1}{R}(v_{C_1} \right. \\ & \left. + -v_{C_2}) + (1-\lambda_2) i_{L_2}\right] - 2(1-\lambda_1)\left[\frac{1}{RC_1}(2v_{C_1} \right. \\ & \left. + -v_{C_2}) i_{L_1} + \frac{V_{in}}{L_1} v_{C_1}\right] + \frac{2}{L_1} V_{in}^2. \end{aligned} \tag{9}$$

From (7), the dynamics of the Boost-1 in terms of z-variables are described by linear model:

$$\dot{\boldsymbol{z}} = \boldsymbol{A}_z \boldsymbol{z} + \boldsymbol{b}_z \mu_1 \tag{10a}$$

$$y_z = z_1 \tag{10b}$$

where:

$$\boldsymbol{A}_z = \begin{bmatrix} 0 & 1 & 0 \\ 0 & 0 & 1 \\ 0 & 0 & 0 \end{bmatrix}, \quad \boldsymbol{b}_z = \begin{bmatrix} 0 \\ 0 \\ 1 \end{bmatrix},$$

$$\mu_1 = \alpha_1 \delta_1 + \eta_1, \tag{11}$$

$$\alpha_1 = \frac{2}{L_1} V_{in} v_{C_1} + \frac{2}{RC_1}(2v_{C_1} - v_{C_2}) i_{L_1}, \tag{12}$$

$$\begin{aligned} \eta_1 = {} & 2\left[-\frac{1}{RC_1}(v_{C_1} - v_{C_2}) + \frac{1}{C_1}(1-\lambda_1) i_{L_1}\right] \\ & \times \left[\frac{1}{R^2 C_1}(4v_{C_1} + -3v_{C_2}) - \frac{2}{RC_1}(1-\lambda_1) i_{L_1} \right. \\ & \left. + \frac{1}{R^2 C_2}(2v_{C_1} - v_{C_2}) + \frac{1}{RC_2}(1 + -\lambda_2) i_{L_2} - \frac{V_{in}}{L_1}(1-\lambda_1)\right] \\ & + 2\left[-\frac{1}{RC_2}(v_{C_2} - v_{C_1}) + \frac{1}{C_2}(1 \right. \\ & \left. + -\lambda_2) i_{L_2}\right]\left[-\frac{1}{R^2 C_1}(3v_{C_1} - 2v_{C_2}) + \frac{1}{RC_1}(1-\lambda_1) i_{L_1} \right. \\ & \left. + -\frac{1}{R^2 C_2} v_{C_1}\right] \\ & - \frac{2}{RC_1 L_1}(1-\lambda_1)\left[V_{in} - (1-\lambda_1) v_{C_1}\right](2v_{C_1} - v_{C_2}) \\ & + \frac{2}{RC_2 L_1}(1-\lambda_2)\left[V_{in} - (1-\lambda_2) v_{C_2}\right] v_{C_1} - \frac{2}{RC_2} v_{C_1} i_{L_2} \dot{\lambda}_2. \end{aligned} \tag{13}$$

α_1 and η_1 represent the control gain and the total disturbance, respectively. Both are nonlinear and time-variant functions of the original state vector, the variable v_{C2} (representing the interaction of Boost-2 on Boost-1), and the circuital parameters.

Model (10) is the Brunovski canonical form of Boost-1 in the z-domain. This transformation is needed to linearize the boost model through a nonlinear state feedback. This feedback allows, under certain conditions, to transform the original nonlinear model of the Boost-1 into a linear model in the z-domain a chain of integrators,

$$\dddot{y}_z = \mu_1. \tag{14}$$

This technique is sensitive to parameter variations, as evident from the complex expressions of α_1 and η_1 in (12) and (13). The main contribution of this paper is to make the controller robust against parameter uncertainties and exogenous disturbances that, unavoidably, would affect the system if the analytic expressions of η_1 and α_1 are considered.

Remark 1: The Brunovsky canonical form (10) has never been presented in literature since it considers the interaction effects between Boost-1 and Boost-2. Indeed, past works considered only isolated DC-DC boost converters, whose canonical form is much simpler. Interestingly, the interaction effects between the two converters can be included in the equivalent disturbance η_1, and the function α_1 does not contain the input variable related to Boost-2. For this reason, an ESO can be designed to estimate the function η_1 as shown

in the following subsection, independently from the control input of Boost-2. ⌟

B. DESIGN OF THE EXTENDED STATE OBSERVER

The ESO is based on model (10), including an extra state variable defined as $z_4 = \eta_1$. The resulting extended model is given by:

$$\dot{\boldsymbol{z}}_e = \boldsymbol{A}_{ze}\boldsymbol{z}_e + \boldsymbol{b}_{ze}\alpha_1\delta_1 + \boldsymbol{b}_{\eta_1}\dot{\eta}_1, \tag{15}$$

where:

$$\boldsymbol{A}_{ze} = \begin{bmatrix} 0 & 1 & 0 & 0 \\ 0 & 0 & 1 & 0 \\ 0 & 0 & 0 & 1 \\ 0 & 0 & 0 & 0 \end{bmatrix}, \ \boldsymbol{z}_e = \begin{bmatrix} z_1 \\ z_2 \\ z_3 \\ z_4 \end{bmatrix}, \ \boldsymbol{b}_{ze} = \begin{bmatrix} 0 \\ 0 \\ 1 \\ 0 \end{bmatrix},$$

$$\boldsymbol{b}_{\eta_1} = \begin{bmatrix} 0 \\ 0 \\ 0 \\ 1 \end{bmatrix}.$$

A Linear ESO (LESO) can be employed to estimate the state $\boldsymbol{z}_e$, as shown below:

$$\dot{\hat{z}}_1 = \hat{z}_2 + \epsilon^{-1}\beta_1 e_z, \tag{16a}$$
$$\dot{\hat{z}}_2 = \hat{z}_3 + \epsilon^{-2}\beta_2 e_z, \tag{16b}$$
$$\dot{\hat{z}}_3 = \hat{z}_4 + \epsilon^{-3}\beta_3 e_z + \alpha_1\delta_1, \tag{16c}$$
$$\dot{\hat{z}}_4 = \epsilon^{-4}\beta_4 e_z, \tag{16d}$$

where the symbol $\hat{}$ denotes the estimated variables, $e_z = z_1 - \hat{z}_1$ is the output estimation error, the parameters β_i, $i = 1, \ldots, 4$ are chosen so that the polynomial

$$s^4 + \beta_4 s^3 + \beta_3 s^2 + \beta_2 s + \beta_1 = 0 \tag{17}$$

is Hurwitz, and ϵ has to be chosen as low as possible, considering that the lower ϵ, the lower the convergence time, the higher the bandwidth of the observer, and the lower the steady-state estimation errors. However, note that the drawback of a small ϵ is a high noise level on the estimated variables, and, consequently, a good compromise between speed of convergence and noise level should be considered.

C. DESIGN OF THE CONTROLLER

The controller design is carried out starting from the Brunovsky canonical form (10), imposing that the output $y_z = z_1 = C_1 v_{C_1}^2 + L_1 i_{L_1}^2$ tracks the desired trajectory. If the boost converter has to work as a DC/DC converter, with output voltage equal to V_{dc}, the reference value of z_1 is perfectly known and given by $z_{1,ref} = C_1 V_{dc}^2 + L_1 I_{dc}^2$, where $I_{dc} = \frac{V_{dc}^2}{R V_{in}}$. A problem arises when the converter has to track a time-varying reference voltage, as in (3), since the real-time reference value of the current is difficult to determine. In the literature, several procedures are shown to determine the inductor current reference; for example, in [3] and [4], it is obtained as the output of a suitably designed high-pass filter; in [1], a systematic procedure is illustrated that allows the determination of the inductor current reference using a differential function of finite order; finally, in [2], the reference state trajectory to be tracked is obtained using the equations of the stable system center, deriving from the ideal internal dynamics, corresponding to a model where these dynamics describes the time evolution of the flat output, i.e. the variable z_1 in the present paper. This paper assumes that the inductor current reference is equal to the measured one, and its derivatives, up to the third order, are estimated by means of a fourth-order differentiator, whose details are given below. This approach is different from that used in [3] and [4] because, for control purposes, the measured current is passed through a differentiator, i.e., a low-pass filter able to reproduce very well the mean waveform of the current itself, canceling at the same time the high-frequency components. In practice, at the start of the sampling period, the inductor current is measured, and the reference variable $z_{1,ref}$ is computed from the value of the reference voltage $y_{1,ref}$ and the measured current. Then, the controller will compute the duty cycle to be applied at the start of the successive sampling interval, following the control law illustrated below in this Section.

1) DESIGN OF THE DIFFERENTIATOR

As already said, the measured current i_{L_1} is applied to a differentiator to compute its derivatives up to the desired order. Here, a linear fourth-order differentiator is considered, described by the following model:

$$\dot{\boldsymbol{\chi}} = \boldsymbol{A}_\chi \boldsymbol{\chi} + p_0 \boldsymbol{h} i_{L_1}, \tag{18}$$

where:

$$\boldsymbol{A}_\chi = \begin{bmatrix} 0 & 1 & 0 & 0 \\ 0 & 0 & 1 & 0 \\ 0 & 0 & 0 & 1 \\ -p_0 & -p_1 & -p_2 & -p_3 \end{bmatrix}, \quad \boldsymbol{h} = \begin{bmatrix} 0 \\ 0 \\ 0 \\ 1 \end{bmatrix}.$$

The parameters p_i, $i = 0, \ldots, 3$, are chosen so that the polynomial

$$s^4 + p_3 s^3 + p_2 s^2 + p_1 s + p_0 = 0 \tag{19}$$

is Hurwitz. The components of $\boldsymbol{\chi}$, χ_1, χ_2, χ_3 and χ_4, represent, respectively, estimates of the current i_{L_1}, $i_{L_1 F}$, and its derivatives $\dot{i}_{L_1 F}$, $\ddot{i}_{L_1 F}$ and $\dddot{i}_{L_1 F}$. The inductor current and its derivatives allow us to compute the derivatives of z_{1ref} as follows:

$$\dot{z}_{1ref} = 2C_1 v_{C_1 ref}\dot{v}_{C_1 ref} + 2L_1 i_{L_1 F}\dot{i}_{L_1 F}, \tag{20a}$$
$$\ddot{z}_{1ref} = 2C_1(\dot{v}_{C_1 ref}^2 + v_{C_1 ref}\ddot{v}_{C_1 ref}) + 2L_1(\dot{i}_{L_1 F}^2 + i_{L_1 F}\ddot{i}_{L_1 F}), \tag{20b}$$
$$\dddot{z}_{1ref} = 2C_1(3\dot{v}_{C_1 ref}\ddot{v}_{C_1 ref} + v_{C_1 ref}\dddot{v}_{C_1 ref}) + 2L_1(3\dot{i}_{L_1 F}\ddot{i}_{L_1 F} + i_{LF}\dddot{i}_{L_1 F}). \tag{20c}$$

2) DESIGN OF THE CONTROL LAW

According to non-linear control theory [28], the control law that stabilizes and assigns the steady-state and dynamic

behavior to a model (14) can be determined as follows:

$$\mu_1 = \ddot{y}_{z,ref} - \gamma_{z2}(\ddot{y}_z - \ddot{y}_{z,ref}) - \gamma_{z1}(\dot{y}_z - \dot{y}_{z,ref}) - \gamma_{z0}(y_z - y_{z,ref}). \quad (21)$$

Indeed, defining $e_{yz} = y_z - y_{z,ref}$, and substituting (21) into (14), the following equation is obtained:

$$\ddot{e}_{yz} + \gamma_{z2}\ddot{e}_{yz} + \gamma_{z1}\dot{e}_{yz} + \gamma_{z0}e_{yz} = 0, \quad (22)$$

which implies that $\lim_{t\to\infty} e_{yz} = 0$ if polynomial $s^3+\gamma_{z2}s^2+\gamma_{z1}s+\gamma_{z0} = 0$ is Hurwitz.

Finally, δ_1 can be derived as follows:

$$\delta_1 = \alpha_1^{-1}(-\eta_1 + \mu_1). \quad (23)$$

However, note that α_1 and η_1 in (23) are known with a certain margin of uncertainty. This consideration suggests modifying the control law (23) by adding a sliding mode (SM) component designed to cope with these uncertainties (cf. [28]). In particular, to gain robustness against parameter deviations and/or variations of the supply DC voltage V_{in} and the load resistance R, the control law in terms of δ_1 is modified as follows:

$$\delta_1 = \frac{1}{\hat{\alpha}_1}(\mu_1 - \hat{\eta}_1 + u_{sm1}), \quad (24)$$

where $\hat{\alpha}_1$ is the nominal value of α_1, $\hat{\eta}_1$ is the estimated value of η_1 by means of ESO, and

$$u_{sm1} = -k_{sm1}\text{sign}(s_1), \quad (25)$$

with:

$$s_1 = \ddot{e}_{yz} + k_1\dot{e}_{yz} + k_0 e_{yz}, \quad (26)$$

and k_{sm1} is a positive constant designed as shown in the following Proposition 1. Before giving the Proposition for determining the gain k_{sm1} the following Assumption 1 is required:

Assumption 1: It is assumed that the maximum error between η_1 and its estimate $\hat{\eta}_1$ is

$$\left|\tilde{\eta}_1\right| = \left|\eta_1 - \hat{\eta}_1\right| \le \epsilon_\eta\left|\hat{\eta}_1\right|, \quad (27)$$

for some positive constant ϵ_η. Moreover, it is assumed that $\alpha_1 \in [\alpha_{1min}, \alpha_{1max}]$ where α_{1min} and α_{1max} are the minimum and the maximum values, respectively, of the control gain α_1 and are obtained assuming deviations of the electric parameters from their nominal ones starting from the tolerances of the components employed for realizing the two converters. In this work, α_{1min} and α_{1max} were chosen considering the 30% tolerance of the circuit components from their nominal values.

Proposition 1: Assuming $\hat{\alpha}_1 = \sqrt{\alpha_{1min}\alpha_{1max}}$ and $\beta = \sqrt{\frac{\alpha_{1max}}{\alpha_{1min}}}$, if the gain k_{sm1} is designed as follows:

$$k_{sm1} \ge |\mu_1 - \hat{\eta}_1| + \beta\epsilon_\eta|\hat{\eta}_1| + \beta|\hat{\eta}_1 + k_1\ddot{e}_{yz1} + k_0\dot{e}_{yz1} - \dddot{y}_{z1ref}|, \quad (28)$$

then the sliding condition is verified, and the system slides on the surface $s_1 = 0$, for each value of the uncertainties satisfying Assumption 1.

Proof: Assuming $\hat{\alpha}_1 = \sqrt{\alpha_{1min}\alpha_{1max}}$ and $\beta = \sqrt{\frac{\alpha_{1max}}{\alpha_{1min}}}$, it follows that

$$\frac{\alpha_1}{\hat{\alpha}_1} \in [\beta^{-1}, \beta], \quad \text{and} \quad \frac{\hat{\alpha}_1}{\alpha_1} \in [\beta^{-1}, \beta]. \quad (29)$$

Substituting (24) into (10), we have:

$$\dot{z}_3 = \left(\eta_1 - \frac{\alpha_1}{\hat{\alpha}_1}\hat{\eta}_1\right) + \frac{\alpha_1}{\hat{\alpha}_1}(\mu_1 - k_{sm1}\,\text{sign}(s_1)). \quad (30)$$

Now, let us define the Lyapunov candidate function as follows:

$$V(s_1) = \frac{1}{2}s_1^2. \quad (31)$$

Computing the derivative of (31) we obtain: $\dot{V}(s_1) = s_1\dot{s}_1$ and, consequently, for obtaining $\dot{V}(s_1) < 0$, the following sliding conditions have to be satisfied:

$$\begin{cases} \dot{s}_1 > 0 & \text{for} \quad s_1 < 0, \\ \dot{s}_1 < 0 & \text{for} \quad s_1 > 0. \end{cases} \quad (32)$$

From (25) and (26), we have:

$$\begin{aligned} \dot{s}_1 &= \dddot{y}_z - \dddot{y}_{z,ref} + k_1(\ddot{y}_z - \ddot{y}_{z,ref}) + k_0(\dot{y}_z - \dot{y}_{z,ref}) \\ &= \tilde{\eta}_1 + \left(1 - \frac{\alpha_1}{\hat{\alpha}_1}\right)\hat{\eta}_1 + \frac{\alpha_1}{\hat{\alpha}_1}(\mu_1 - k_{sm1}\text{sign}(s_1)) \\ &\quad + k_1(\ddot{y}_z - \ddot{y}_{z,ref}) + k_0(\dot{y}_z - \dot{y}_{z,ref}) - \dddot{y}_{z,ref}. \end{aligned} \quad (33)$$

Then, from (32), it is obtained that:

$$\begin{aligned} &\tilde{\eta}_1 + \left(1 - \frac{\alpha_1}{\hat{\alpha}_1}\right)\hat{\eta}_1 + \frac{\alpha_1}{\hat{\alpha}_1}(\mu_1 - k_{sm1}) + k_1(\ddot{y}_z - \ddot{y}_{z,ref}) \\ &\quad + k_0(\dot{y}_z - \dot{y}_{z,ref}) - \dddot{y}_{z,ref} < 0, \quad \text{for } s > 0, \end{aligned} \quad (34)$$

$$\begin{aligned} &\tilde{\eta}_1 + \left(1 - \frac{\alpha_1}{\hat{\alpha}_1}\right)\hat{\eta}_1 + \frac{\alpha_1}{\hat{\alpha}_1}(\mu_1 + k_{sm1}) + k_1(\ddot{y}_z - \ddot{y}_{z,ref}) \\ &\quad + +k_0(\dot{y}_z - \dot{y}_{z,ref}) - \dddot{y}_{z,ref} > 0, \quad \text{for } s < 0, \end{aligned} \quad (35)$$

both of which are satisfied for:

$$k_{sm1} > \max_{\tilde{\eta}_1,\alpha_1}\left|\mu_1 - \hat{\eta}_1 + \frac{\hat{\alpha}_1}{\alpha_1}\left(\tilde{\eta}_1 + \hat{\eta}_1 + k_1(\ddot{y}_z - \ddot{y}_{z,ref}) + k_0(\dot{y}_z - \dot{y}_{z,ref}) - \dddot{y}_{z,ref}\right)\right|. \quad (36)$$

Using the conditions given in Assumption 1, (36) can be maximized ad follows:

$$\begin{aligned} &\left|\mu_1 - \hat{\eta}_1 + \frac{\hat{\alpha}_1}{\alpha_1}\left(\tilde{\eta}_1 + \hat{\eta}_1 + k_1(\ddot{y}_z - \ddot{y}_{z,ref}) + k_0(\dot{y}_z - \dot{y}_{z,ref}) - \dddot{y}_{z,ref}\right)\right| \le \left|\mu_1 - \hat{\eta}_1\right| + \frac{\hat{\alpha}_1}{\alpha_1}\left|\tilde{\eta}_1\right| + \frac{\hat{\alpha}_1}{\alpha_1}\left|\hat{\eta}_1 + k_1(\ddot{y}_z - \ddot{y}_{z,ref}) \right. \\ &\left. + k_0(\dot{y}_z - \dot{y}_{z,ref}) - \dddot{y}_{z,ref}\right| \le \left|\mu_1 - \hat{\eta}_1\right| + \beta\epsilon_\eta\left|\hat{\eta}_1\right| \\ &+ \beta\left|\hat{\eta}_1 + k_1(\ddot{y}_z - \ddot{y}_{z,ref}) + k_0(\dot{y}_z - \dot{y}_{z,ref}) - \dddot{y}_{z,ref}\right|. \end{aligned} \quad (37)$$

From (37) follows that (32) is satisfied if k_{sm1} is as shown in (28). This concludes the proof. ⌟

Remark 2: Note that condition (36) does not depend on the electromagnetic parameters as it occurs, for example, in [8]. This is important because it is challenging to verify a priori if the sliding conditions are satisfied for all the values of the parameters in the cases where they depend on the parameters themselves. ⌟

Remark 3: From the Proof III-C2, it is evident that two procedures can be followed to satisfy condition (36). The first consists of estimating an upper bound of k_{sm1}, which satisfies the sliding condition in all the possible operating situations. The second is to select, online, the time-variant gain k_{sm1}, computing the second member of (28), including β, which is computed as indicated in Proposition 1, considering the maximum and minimum values for the electromagnetic parameters, and assuming that the measured voltages and currents are not affected by errors. The first choice is too conservative and results in an increase in chattering. The second choice has been adopted in this work. Moreover, it is helpful to note that even if the gain is time-varying, it does not depend on the particular values of α_1 or η_1, which are unknown. Instead, only the value of ϵ_η has to be chosen because the other variables in (28) are computed online. ⌟

Remark 4: It is important to note that, in contrast with [2] where the coordinate transformation leads to a canonical form nonlinear model having an internal dynamics unstable of order 1, the coordinate transformation used here leads to a linear model having no internal dynamics. ⌟

As highlighted at the beginning of this Section, the same controller illustrated for Boost-1 will be applied to Boost-2, which is omitted for this reason.

The block diagram of the proposed control technique is shown in Fig. 2.

Remark 5: Note that the proposed control law is not influenced by the power range of the converter; therefore, there are no limitations and it can be employed both in low-power and high-power applications. ⌟

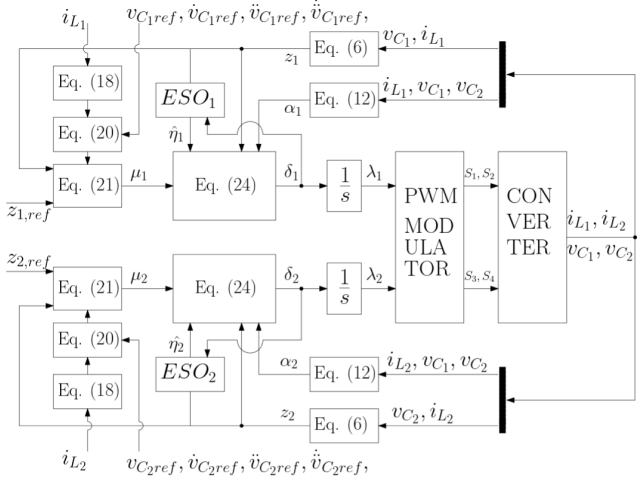

FIGURE 2. Block diagram of the proposed control technique.

IV. SIMULATION RESULTS

In order to validate the controller previously illustrated, simulation experiments are carried out using an implementation of the plant and the controller in the Matlab-Simscape environment.

In order to test the behavior of the boost inverter and its robustness against input voltage and load variations, a test is carried out considering nominal converter parameters. In particular, at $t = 0.1$, two sinusoidal voltage references with 50 Hz of frequency and 40 V of amplitude are imposed on both the converters, according to (3) and (4) (with $V_{dc} = 110$V), in order to generate a sinusoidal differential output voltage of amplitude 80 V. Then, a step variation of -12.5% in the input voltage is imposed at the instant 0.3 s. Finally, at the instant 0.4 s, a variation of the load resistance, equal to -50%, is applied, restoring, at the same time, the nominal input voltage. Finally, at $t = 0.5$ s, the reference voltage is set at zero.

The parameters of the boost inverter are given in Table 1. From the data sheets of the inductors and capacitors, the maximum value deviations are $\pm 20\%$ for the inductance and $\pm 10\%$ for the capacitance. The parameters of the controller are chosen such that:

- *Controller:* the roots of polynomial (22) are real, negative and equal to $\omega_{contr} = 10150$ rad/s;
- *ESO:* the roots of polynomial (17) are real, negative and equal to $\omega_{eso} = 100$ rad/s;
- *Differentiator:* the roots of polynomial (19) are real, negative and equal to $\omega_{diff} = 20000$ rad/s;
- *Sliding function:* the roots of polynomial (26) are real, negative and equal to $\omega_{sl} = 1000$ rad/s;

The simulation results are shown in Figs. 3-7. These results show that the differential boost inverter can generate a sinusoidal voltage with a maximum amplitude error of 0.65% in all situations. The harmonic content of the output voltage consists of odd harmonics, with the third harmonics, the bigger one, about 1% of the fundamental frequency, and a fifth harmonics less than 0.4%. The total harmonic distortion (THD) depends on the bandwidth of the differentiator and, in this test, is equal to 2.05%.

The currents have not a sinusoidal waveform due to the nonlinear characteristic of the boost converters, and their peak-to peak value increases to compensate for the variations of the input voltage and load. As already said, the measured inductor currents assume the significance of reference currents and, consequently, it is possible to generate the reference variable z_{1ref} and the state variable z_1, both useful for the control loop of the feedback-linearized system. Figure 6 shows the tracking high capability of this control loop, where the state variable is superimposed to the reference one. Finally, Fig. 7 shows the high capability of the ESO in the estimation of the state variable z_1, which is a necessary condition for a good estimation of the total disturbance η_1,

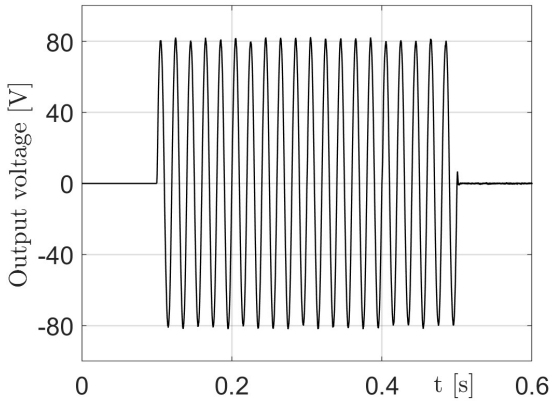

FIGURE 3. Output voltage generated during the test with nominal parameters.

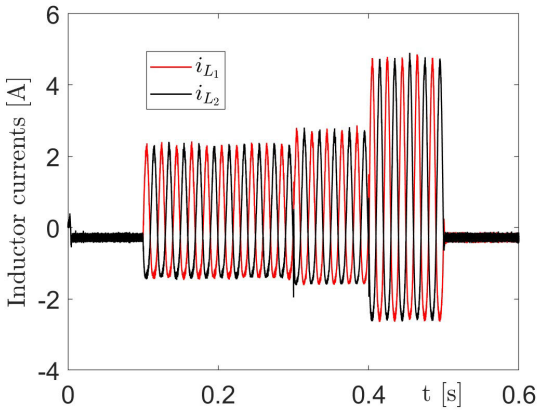

FIGURE 4. Currents in the inductors of the two boost converters, generated during the test with nominal parameters.

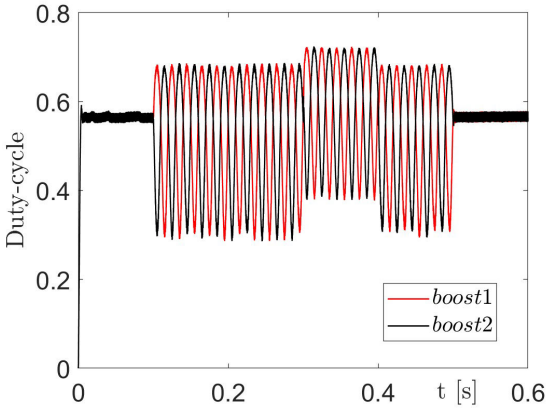

FIGURE 5. Duty cycles generated during the test with nominal parameters.

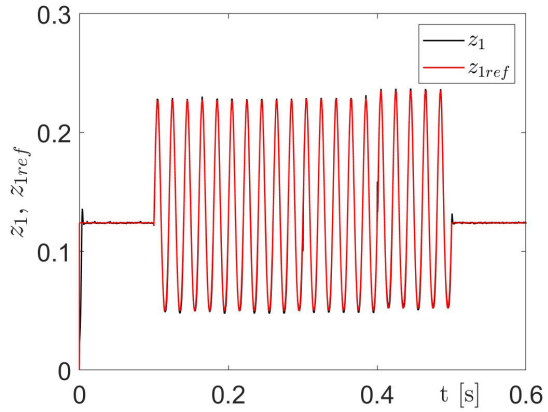

FIGURE 6. Reference variable z_{1ref} and variable z_1 generated during the test with nominal parameters.

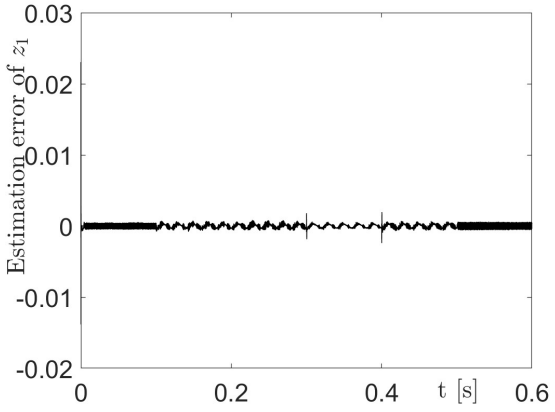

FIGURE 7. Estimation error of the variable z_1 generated from the ESO 1 during the test with nominal parameters.

useful in the computation of δ_1 and then of the duty-cycle λ_1. It is worthwhile to observe the smooth waveforms of the duty cycles due to the presence of the dynamic input, which in turn produces smooth forms into the voltages v_{C_1} and v_{C_2}, and then in the output voltage, by avoiding the main issue of other standard sliding mode controllers. Finally, the results described in this test show that the output voltage is practically insensitive to input voltage variations and load resistance variations. Naturally, the inductor currents vary in the presence of the above variations, as illustrated in Fig. 4.

Since one strength of the proposed algorithm is its robustness against electrical parameter variations, to demonstrate the performance of the proposed control technique, a second test was carried out by imposing a strong mismatch of the two boosts parameters. In particular, the values of L_1, L_2, C_1, and C_2 are varied with an increment of 30% for the Boost-1 and a decrement of 30% for the Boost-2. Moreover, the parasitic resistances of both inductances and capacitors were considered in the circuit. The type of test in terms of reference output voltage and input and load variations is the same as the previous one shown in Figs. 3-4. The simulation results are given in Figs. 8 and 9. Examination of these figures shows that the robustness of the output voltage is maintained for variations of input voltage and load resistance, whereas a mismatch of the inductor currents appears. In particular, peak values of the current i_{L_1} diminish, whereas that of i_{L_2} increase. The total harmonic distortion, equal to 2.92%, increases slightly compared with the test with nominal parameters, but

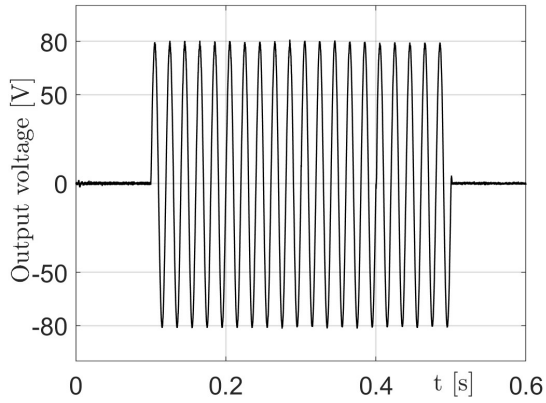

FIGURE 8. Output voltage generated during a test with strong parameters variation.

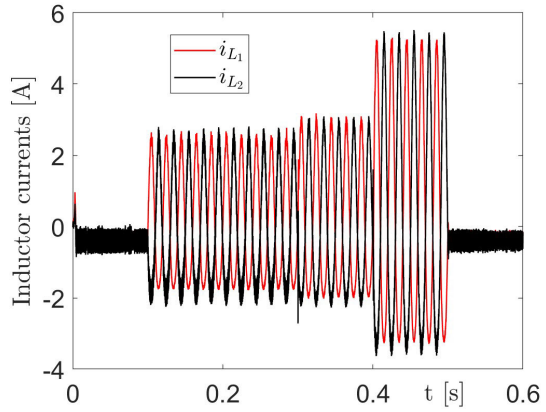

FIGURE 9. Currents in the inductors of the two boost converters, generated during a test with strong parameters variation.

it is widely acceptable. This benefit is due to the proposed approach since the equivalent disturbance is estimated and compensated online, and the sliding mode action allows it to gain robustness against possible exogenous disturbances and input errors of the ESOs, thus confirming the effectiveness of the proposed approach.

V. EXPERIMENTAL SETUP

This section presents the experimental setup suitably built to validate the proposed controller. The converter under test is shown in Fig.1 while in Fig.10, a photo of the overall test bench is given. Moreover, Table 1 shows the components and their values used to conduct the experiments. The controller has been implemented on the F28379D LaunchPad development kit for the C2000 Delfino MCU by Texas Instrument, a low-cost evaluation and development board for the TMS320F28379D microcontroller. The board features a 32-bit microcontroller with a dedicated coprocessor for optimizing floating point calculations, the CLA (Control Law Accelerator).

The processor, in particular features a dual-core architecture with two C28x CPUs and two CLAs, operating

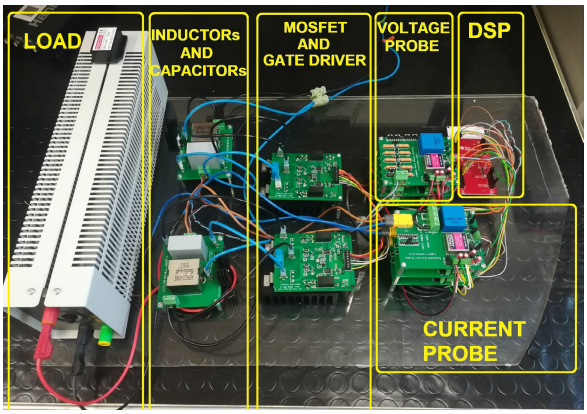

FIGURE 10. Photo of the overall test setup.

TABLE 1. Parameters of the converter.

NAME	VALUE	COMPONENT	BRAND	DESCRIPTION
V_{IN}	48V			Input Voltage
R	100Ω	VRH320 100R K	Arcol	Load Resistor
$L_{1,2}$	470μH	AGP4233-474ME	Coilcraft	Inductors
$C_{1,2}$	10μF	MKP1848610094P	Vishay	Capacitors
$S_{1,2,3,4}$	-	SCTWA90N65G2V	ST	Switch
$Driver$	-	STGAP2SCIC	ST	Switch Driver

at 200 MHz with a total processing capability of 800 MIPS. It includes 1024 kB of flash memory, 204 kB of RAM, and supports advanced functionalities such as 12- and 16-bit ADC resolution, 24 PWM channels, and 8 SPI interfaces.

In particular, the implementation has been made so that the CLA executes the control algorithm at 100khz. In contrast, other tasks, which do not need to be executed with strict timings, are executed on the main CPU. The source files necessary for implementing the algorithm have been developed employing Matlab-Simulink software.

The MOSFETs' gates are logically driven through the PWM generator modules available on the processor. Specific attention has been given to the design of the driver circuitry using the STGAP2SICS driver from ST-Microelectronics. In particular the implementation follows the application diagram with Miller Clamp and negative gate driving as shown in [29, Fig. 10, page 12/22]. The Miller clamp function allows control of the Miller current during power stage switching in half-bridge configurations. When the external power transistor is in the OFF state, the driver operates to avoid the induced turn-on phenomenon that may occur when the other switch in the same leg is being turned on. During the turn-off period, the gate of the external switch is monitored through the CLAMP pin. The CLAMP switch is activated when the gate voltage goes below the voltage threshold, thus creating a low impedance path between the switch gate and the GNDISO pin (please refer to [29, Fig. 10, page 12/22] for this description).

To measure the system state, specifically the voltages on the output capacitors V_{C1}, V_{C2} and the currents through the inductors i_{L1} and i_{L2}, some LA 25-NP LEM Hall

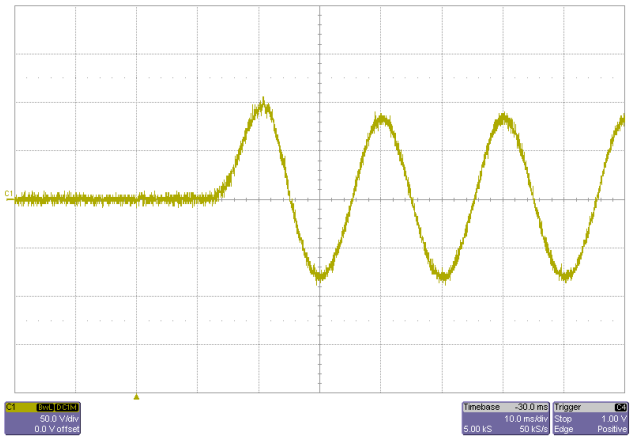

FIGURE 11. Output voltage v_o during a start-up sequence.

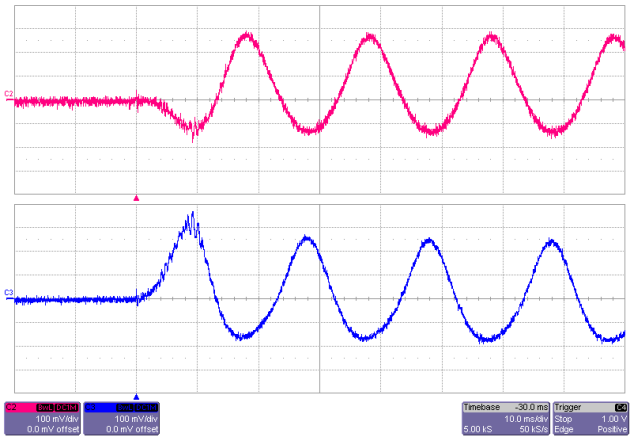

FIGURE 12. Inductor currents i_{L1} (purple) and i_{L2} (blue) during a start-up sequence.

effect sensors were used. These sensors were installed on custom boards built explicitly for the implementation of this experimental setup. All signals are sampled and converted by the four parallel on-board analog to digital converters. For acquisition via oscilloscope, and to generate the graphs related to the experimental tests, two Teledyne T3CP100-2 current probes, configured with 0.1V/A scale, and two Tektronix P5200 voltage probes, were used in conjuction with the Lecroy Wavepro 7200A DSO. A digital pin on the CPU was also used to trigger the startup sequence and the load and voltage variation tests.

VI. EXPERIMENTAL RESULTS

In this section, experimental results are given. In particular, a start-up test, a steady-state test, and a load variation test were performed in order to validate the effectiveness of the proposed control technique.

A start-up test shows the system's behavior in a start-up sequence, i.e., the initial transient, in which it starts from zero and generates a sine wave with a peak-to-peak amplitude of 160V and a frequency of 50 Hz. In particular, the results of this test are shown in Figs. 11 and 12. Fig. 11 shows

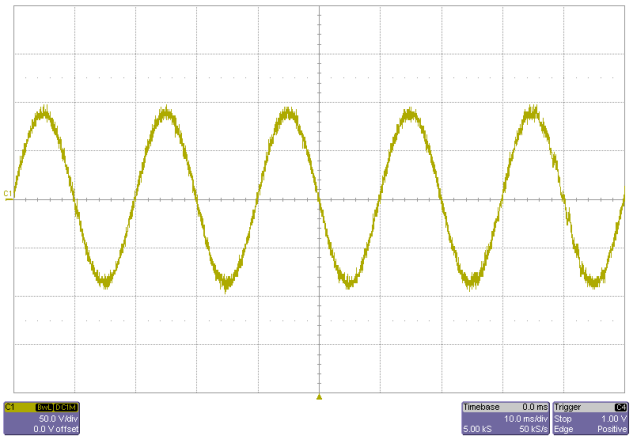

FIGURE 13. Output voltage v_o in a steady-state operating condition.

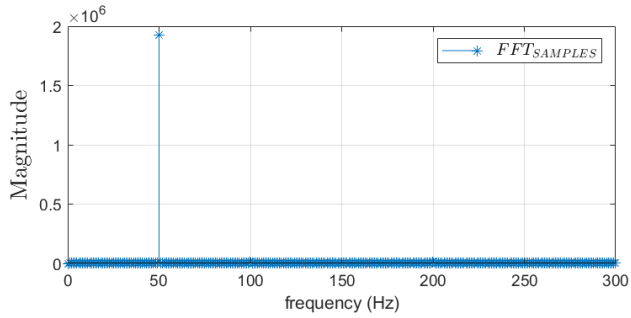

FIGURE 14. FFT samples in a steady-state operating condition.

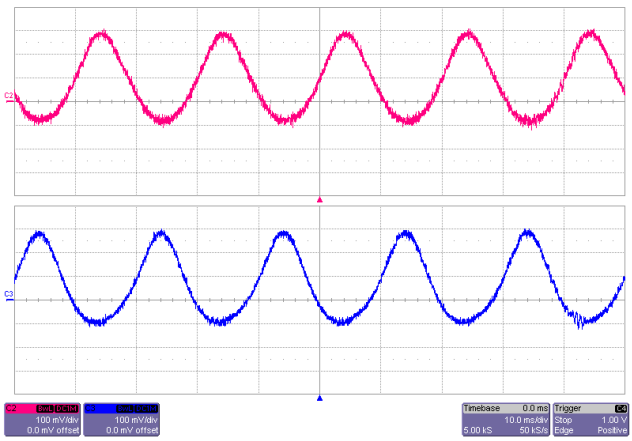

FIGURE 15. Inductor currents i_{L1} (purple) and i_{L2} (blue) in steady-state operating condition.

the waveform of the output voltage v_o while Fig. 12 shows the i_{L1} and i_{L2} inductor currents trends. These results show that the system perfectly tracks the sinusoidal reference, the overshoot is negligible, and the steady state is reached after less than 50 milliseconds.

The steady-state test results are shown in Figs.13-15. In particular, Fig. 13 shows the waveform of the output voltage v_o in a steady-state condition while in Fig.14 the FFT components were reported. In Fig.15, the waveforms of the

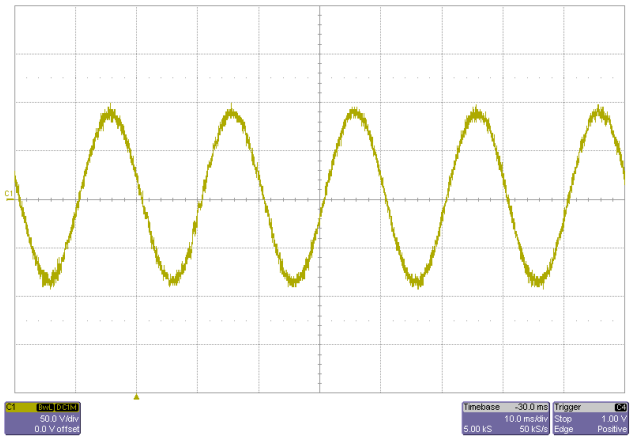

FIGURE 16. Output voltage v_o in a load variation transient.

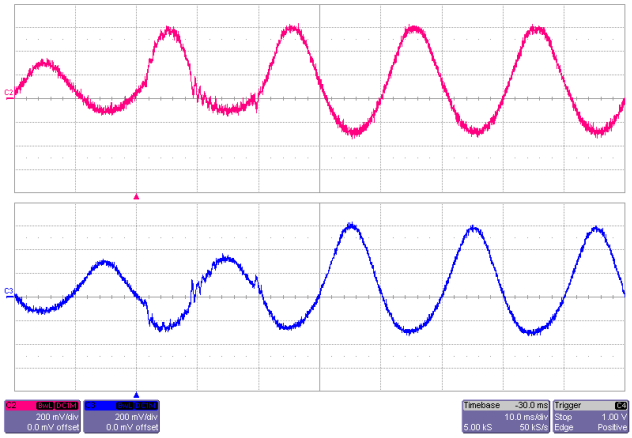

FIGURE 17. Inductor currents i_{L1} (purple) and i_{L2} (blue) in a load variation transient.

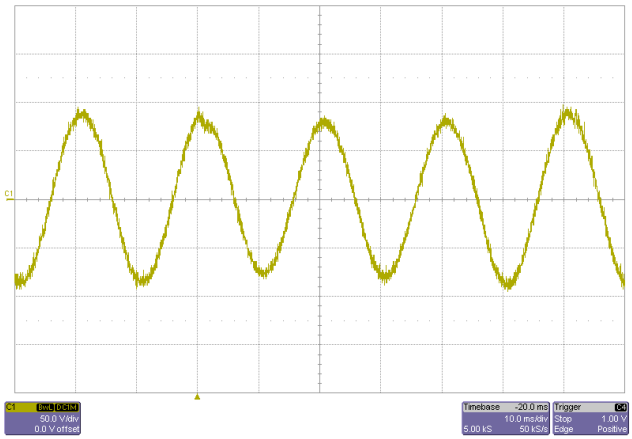

FIGURE 18. Output voltage v_o in an input voltage variation transient.

inductor currents i_{L1} and i_{L2} are shown for the same operating conditions. It can be seen from these tests that the system can follow correctly the sinusoidal reference. Furthermore, in this test, the FFT was performed. From the results shown in Fig.14, it is possible to see that there is a negligible distortion

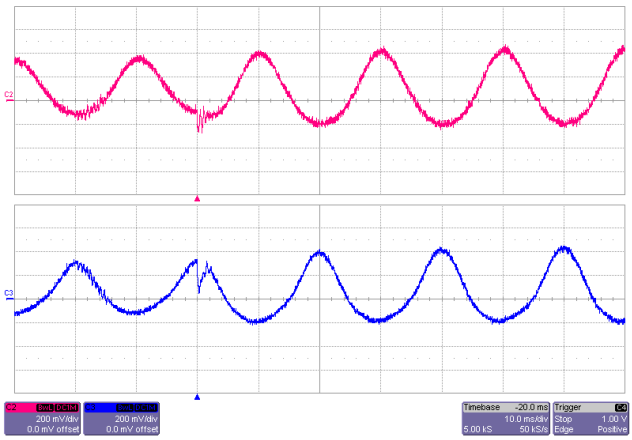

FIGURE 19. Inductor currents i_{L1} (purple) and i_{L2} in an input voltage variation transient.

with the third harmonics about 1.3% of the fundamental frequency, and a fifth harmonics less than 0.5%. The total harmonic distortion (THD) is equal to 2.45%.

A load variation test was also carried out. The load resistance R was changed from an initial value of 100 Ω to a final value of 50 Ω. The results are shown in Figs.16-17, where the waveforms of the output voltage v_o and inductor currents i_{L1} and i_{L2} are shown during a load variation. It can be seen from this test that the control system can reject the disturbance; in fact, the output voltage v_o is not affected by load variation, i.e., the influence on v_o is negligible, and the inductor currents i_{L1} and i_{L2} rise instantaneously, as can be seen from Fig. 17, coherently with the load variation.

Finally, an input voltage variation test was performed by decreasing the input voltage v_{in} from the nominal 48V value to 42V. Results are shown in Figs.18-19. Also, the output voltage is almost insensible to input voltage variations, and the currents attain their steady-state values quickly.

In all cases, the experimental results are coherent with the simulations given in Section IV. Indeed, by examination of the figures, the same current values are obtained, and almost the same THD is gained (2.45% in the experimental results and 2.05% in the simulations) by validating the congruence between simulations and experiments.

VII. CONCLUSION

This work addresses the control of a differential boost inverter for DC/AC operations. In particular, a rigorous procedure is shown to put the system in Brunovski's canonical form and to derive suitable developed ESOs to compensate for nonlinear disturbances. A sliding mode component was designed to ensure the robustness of the whole closed-loop system against supply voltage and load variations. Moreover, to avoid the chattering problem, a model with dynamic inputs was used, where the control variables are the duty cycles of the two boost converters, and they are obtained as the integrals of two auxiliary inputs. This choice implies that the control variables are not affected by chattering.

Simulation experiments showed that the closed-loop system could generate sinusoidal voltages, and the controller was found to be particularly robust against both exogenous and endogenous disturbances. Experimental results are congruent with those obtained by simulations, showing that the system works well and can effectively reject load and input voltage variation disturbances. Moreover, the reproduced waveforms are good, with negligible harmonic distortion, which confirms the effectiveness of the proposed algorithm.

ACKNOWLEDGMENT

The authors thank TopNetwork SpA for supporting this research.

REFERENCES

[1] H. Sira-Ramirez, "Flatness and trajectory tracking in sliding mode based regulation of DC-to-AC conversion schemes," in *Proc. 38th IEEE Conf. Decis. Control*, vol. 5, Dec. 1999, pp. 4268–4273.

[2] Y. B. Shtessel, A. S. I. Zinober, and I. A. Shkolnikov, "Sliding mode control of boost and buck-boost power converters using method of stable system centre," *Automatica*, vol. 39, no. 6, pp. 1061–1067, Jun. 2003.

[3] R. Caceres and I. Barbi, "A boost DC–AC converter: Operation, analysis, control and experimentation," in *Proc. 21st Annu. Conf. IEEE Ind. Electron. (IECON)*, Nov. 1995, pp. 546–551.

[4] P. Sanchis, A. Ursæa, E. Gubía, and L. Marroyo, "Boost DC–AC inverter: A new control strategy," *IEEE Trans. Power Electron.*, vol. 20, no. 2, pp. 343–353, Mar. 2005.

[5] S.-W. Seo and H. H. Choi, "Digital implementation of fractional order PID-type controller for boost DC–DC converter," *IEEE Access*, vol. 7, pp. 142652–142662, 2019.

[6] L. F. D. S. C. Pereira, E. Batista, M. A. G. de Brito, and R. B. Godoy, "A robustness analysis of a fuzzy fractional order PID controller based on genetic algorithm for a DC–DC boost converter," *Electronics*, vol. 11, no. 12, p. 1894, Jun. 2022.

[7] K. Jha, S. Mishra, and A. Joshi, "High-quality sine wave generation using a differential boost inverter at higher operating frequency," *IEEE Trans. Ind. Appl.*, vol. 51, no. 1, pp. 373–384, Jan. 2015.

[8] R. O. Caceres and I. Barbi, "A boost DC–AC converter: Analysis, design, and experimentation," *IEEE Trans. Power Electron.*, vol. 14, no. 1, pp. 134–141, Jan. 1999.

[9] D. Cortes, N. Vazquez, and J. Alvarez-Gallegos, "Dynamical sliding-mode control of the boost inverter," *IEEE Trans. Ind. Electron.*, vol. 56, no. 9, pp. 3467–3476, Sep. 2009.

[10] F. Flores-Bahamonde, H. Valderrama-Blavi, J. M. Bosque-Moncusi, G. García, and L. Martínez-Salamero, "Using the sliding-mode control approach for analysis and design of the boost inverter," *IET Power Electron.*, vol. 9, no. 8, pp. 1625–1634, Jun. 2016.

[11] D. Lopez-Caiza, F. Flores-Bahamonde, S. Kouro, V. Santana, N. Müller, and A. Chub, "Sliding mode based control of dual boost inverter for grid connection," *Energies*, vol. 12, no. 22, p. 4241, Nov. 2019.

[12] Q. Qi, D. Ghaderi, and J. M. Guerrero, "Sliding mode controller-based switched-capacitor-based high DC gain and low voltage stress DC–DC boost converter for photovoltaic applications," *Int. J. Electr. Power Energy Syst.*, vol. 125, Feb. 2021, Art. no. 106496.

[13] R. N. Deo, A. Shrivastava, and K. Chatterjee, "Implementation of sliding mode backstepping controller for boost converter in real-time for LED application," *Expert Syst.*, vol. 40, no. 6, Jul. 2023, Art. no. e13095.

[14] F. Mohammadhassani and H. G. Narm, "Dynamic sliding mode control of single-stage boost inverter with parametric uncertainties and delay," *IET Power Electron.*, vol. 14, no. 12, pp. 2127–2138, Sep. 2021.

[15] R. Musona and I. Serban, "Differential single-phase inverters with active power decoupling: A survey," *IEEE Access*, vol. 11, pp. 53654–53670, 2023.

[16] S.-C. Tan, Y. M. Lai, and C. K. Tse, "Implementation of pulse-width-modulation based sliding mode controller for boost converters," *IEEE Power Electron Lett.*, vol. 3, no. 4, pp. 130–135, Dec. 2005.

[17] A. Isidori, *Nonlinear Control Systems*. Berlin, Germany: Springer, 2013.

[18] S. Ahmad and A. Ali, "Active disturbance rejection control of DC–DC boost converter: A review with modifications for improved performance," *IET Power Electron.*, vol. 12, no. 8, pp. 2095–2107, Jul. 2019.

[19] S. Zhuo, A. Gaillard, L. Guo, L. Xu, D. Paire, and F. Gao, "Active disturbance rejection voltage control of a floating interleaved DC–DC boost converter with switch fault consideration," *IEEE Trans. Power Electron.*, vol. 34, no. 12, pp. 12396–12406, Dec. 2019.

[20] X. Zhou, Q. Liu, Y. Ma, and B. Xie, "DC-link voltage research of photovoltaic grid-connected inverter using improved active disturbance rejection control," *IEEE Access*, vol. 9, pp. 9884–9894, 2021.

[21] H. Yuan and Y. Kim, "Compensated active disturbance rejection control for voltage regulation of a DC–DC boost converter," *IET Power Electron.*, vol. 14, no. 2, pp. 432–441, Feb. 2021.

[22] H. Li, X. Liu, and J. Lu, "Research on linear active disturbance rejection control in DC/DC boost converter," *Electronics*, vol. 8, no. 11, p. 1249, Oct. 2019.

[23] H. Zhang, H. Xiong, and C. He, "Research on active disturbance rejection based on new single-stage buck-boost inverter," in *Proc. IEEE 3rd Student Conf. Electr. Mach. Syst. (SCEMS)*, Dec. 2020, pp. 751–755.

[24] H. Zhang, R. Ma, C. Han, R. Xie, B. Liang, and Y. Li, "Advanced control design of interleaved boost converter for fuel cell applications," in *Proc. IECON 46th Annu. Conf. IEEE Ind. Electron. Soc.*, Oct. 2020, pp. 5000–5005.

[25] S. Zhuo, A. Gaillard, L. Xu, H. Bai, D. Paire, and F. Gao, "Enhanced robust control of a DC–DC converter for fuel cell application based on high-order extended state observer," *IEEE Trans. Transport. Electrific.*, vol. 6, no. 1, pp. 278–287, Mar. 2020.

[26] R. D. Middlebrook and S. Cuk, "A general unified approach to modelling switching-converter power stages," in *Proc. IEEE Power Electron. Spec. Conf.*, Jun. 1976, pp. 18–34.

[27] O. Gehan, E. Pigeon, T. Menard, M. Pouliquen, H. Gualous, Y. Slamani, and B. Tala-Ighil, "A nonlinear state feedback for DC/DC boost converters," *J. Dyn. Syst., Meas., Control*, vol. 139, no. 1, Jan. 2017, Art. no. 011010.

[28] J.-J. E. Slotine and W. Li, *Applied Nonlinear Control*. Englewood Cliffs, NJ, USA: Prentice-Hall, 1991.

[29] STMicroelectronics. (Sep. 2022). *Galvanically Isolated 4 A Single Gate Driver for SiC MOSFETs*. [Online]. Available: https://www.st.com/resource/en/datasheet/stgap2sics.pdf

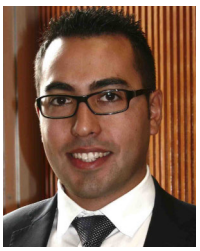

ANTONINO SFERLAZZA (Senior Member, IEEE) was born in Palermo, Italy, in 1987. He received the master's degree in automation engineering and the Ph.D. degree in mathematics and automation from the University of Palermo, Italy, in 2011 and 2015, respectively. In 2013, he was a Visiting Ph.D. Student at the University of California at Santa Barbara, CA, USA, involved in the field of modeling and analysis of stochastic hybrid systems. From 2016 to 2017, he joined the University of Palermo, as a Junior Researcher. From 2017 to 2018, he was a Researcher with LAAS-CNRS, Toulouse, France, involved in the field of power converter control. He is currently a Researcher of systems and control engineering with the University of Palermo. His research interests include the development of feedback control algorithms for nonlinear dynamical systems, optimization techniques, estimation of stochastic dynamical systems, and applications of control of electrical drives, power converters, and mechanical systems. He is a member of the Technology Conferences Editorial Board of the IEEE Control System Society. He serves as an Associate Editor for *European Journal of Control* (Elsevier).

SILVIA DI GIROLAMO (Student Member, IEEE) was born in Marsala, Italy, in December 1998. She received the master's degree in electronics engineering from the University of Palermo, Palermo, Italy, in 2022, where she is currently pursuing the Ph.D. degree in autonomous systems.

Her research interests include hybrid dynamic systems and their applications to sustainable mobility. She is also interested on the control of power converters and electrical drives.

GIOVANNI GARRAFFA (Member, IEEE) was born in Palermo, Italy, in May 1986. He received the Ph.D. degree in energy and information technology engineering from the University of Palermo, in July 2021.

He is currently a Researcher with the Department of Engineering and Architecture, Kore University of Enna. His research interests include the development of algorithms for indoor vehicle localization and autonomous flight and power converters. He is also interested on the development of testing platform to evaluate control algorithm performances.

FRANCESCO ALONGE (Life Member, IEEE) was born in Agrigento, Italy, in 1946. He received the Laurea degree in electronic engineering from the University of Palermo, in 1972. Since 1972, he has been with the University of Palermo, where he is currently a Full Professor of automatic control with the Department of Systems and Control Engineering. His research interests include electrical drive control (including linear and nonlinear observers, stochastic observers, and parametric identification), robot control, parametric identification and control in power electronics, and UAV motion control in aeronautics.

IVAN MARCHESE was born in Palermo, Italy, in 1987. He received the master's degree in mechanical engineering from the University of Palermo, Italy, in 2017, where he is currently pursuing the Ph.D. degree in information and communication technologies with the Department of Engineering.

He has been a Lecturer of PLC, engineer automation, SCADA systems, ICT, smart grids, electronics, and electrotechnics at various public technical institutes in Palermo, and national and international companies (Brembo S.p.A. and Procter and Gamble). His research interests include the development of feedback control algorithms for nonlinear dynamical systems and applications of control of electrical drives, power converters, and mechanical systems.

VINCENZO LEONARDI was born in Palermo, Italy, in 1978. He received the master's degree in information engineering from Guglielmo Marconi University, Rome, Italy, in 2016.

From 2000 to 2012, he was a Researcher of private research and development industrial in telecommunication embedded systems. From 2012 to 2023, he was a Researcher of private research and development industrial in IoT embedded systems. He is currently the Project Manager and the Research and Development Laboratory Manager of IoT and ML systems with TopNetwork SpA, Palermo. His research interests include the optimization of IoT architecture, the standardization of protocol communication from devices to EDGE and cloud systems, and the potential of ML applied to the IoT world for the analysis of large amounts of data.

FRANCESCO MARIA RAIMONDI was born in Palermo, Italy, in 1969. He received the Laurea degree (cum laude) in electrical engineering and the Ph.D. degree in control engineering from the University of Palermo, in 1993 and 1998, respectively. He has been teaching industrial SCADA automation systems and domotics and the fundamentals of automatic control, since 1999 and since 2022, respectively. In 2014, he founded the System and Marine Technologies Laboratory and the LaSiTecMa-Laboratory, and in 2017, he was one of the founders and the CEO of EngCoSys Srl, an innovative start-up and spin-off of the University of Palermo. His scientific research interests include PLCs, nautical drones, domotics and building control systems, SCADA-HMI, and industrial controllers.

FILIPPO D'IPPOLITO (Senior Member, IEEE) was born in Palermo, Italy, in 1966. He received the Laurea degree in electronic engineering and the Research Doctorate degree in systems and control engineering from the University of Palermo, in 1991 and 1996, respectively.

He is currently an Associate Professor with the Department of Engineering, University of Palermo. His research interests include control of electrical drives, control of electrical power converters, adaptive and visual/force control of robot manipulators, rehabilitation robotics, and marine robotics. He received the 2000 Kelvin Premium from the Institution of Electrical Engineers (IEE), for the paper: Parameter identification of induction motor model using genetic algorithms.

Open Access funding provided by 'Università degli Studi di Enna "KORE"' within the CRUI CARE Agreement